Determining PV Penetration for Distribution Systems With Time-Varying Load Models

Duong Quoc Hung, *Student Member, IEEE*, Nadarajah Mithulananthan, *Senior Member, IEEE*, and Kwang Y. Lee, *Fellow, IEEE*

***Abstract*—A constant or voltage-dependent load model is usually assumed in most distributed generation (DG) planning studies. However, this paper proposes several different types of time-varying voltage-dependent load models to determine the penetration level of photovoltaic (PV) units in a distribution network. Here, a new analytical expression is first proposed to size a PV unit, which can supply active and reactive powers. This expression is based on the derivation of a multiobjective index (IMO) that is formulated as a combination of three indices, namely active power loss, reactive power loss and voltage deviation. The expression is then adapted to allocate PV units while considering the time-varying load models and probabilistic PV generation. The effectiveness of the proposed approach was validated on 69- and 33-bus test distribution systems. The results showed that PV allocation with different types of time-varying load models can produce dissimilar penetration levels.**

***Index Terms*—Distributed power generation, loss reduction, multiobjective index, photovoltaic (PV) penetration, PV systems, power generation planning, power system planning, solar energy, time-varying load model, voltage deviation.**

I. Introduction

DUE to economical and environmental benefits and governmental incentives, there has been increased interest in the usage of alternative renewable energy such as biomass, wind and solar worldwide. As of 2010, renewable energy supplied 16.7% of the global energy consumption [1]. Among all renewable energy technologies, solar photovoltaic (PV) grew fastest with a yearly increase of 58% during the period of late 2006 to 2011 [1] and achieved just over 102 GW of the cumulative global installed capacity in 2012 [2]. It is expected that this figure could increase to more than 420 GW in 2017 [2]. Depending on the location and technology of PV adopted, a power system would accommodate up to an estimated 50% of the PV penetration [3], [4]. However, the time-varying load model (i.e., time-varying voltage-dependent load model) may diversely affect the estimated PV penetration.

Manuscript received November 01, 2013; revised February 05, 2014; accepted March 24, 2014. Paper no. TPWRS-01394-2013.

D. Q. Hung and N. Mithulananthan are with the School of Information Technology and Electrical Engineering, University of Queensland, Brisbane, Qld. 4072, Australia (e-mail: hung.duong@uq.edu.au; mithulan@itee.uq.edu.au).

K. Y. Lee is with the Department of Electrical and Computer Engineering, Baylor University, Waco, TX 76798-7356 USA (e-mail: Kwang_Y_Lee@baylor.edu).

Color versions of one or more of the figures in this paper are available online at http://ieeexplore.ieee.org.

Digital Object Identifier 10.1109/TPWRS.2014.2314133

The multiobjective optimization for DG planning considering the active and reactive power losses and voltage deviation has been reported in [5]–[7]. Although well suited for placing dispatchable sources such as gas turbines, such planning studies have not addressed a practical scenario considering the variant demand and nondispatchable renewable generation. Recently, a few studies on renewable DG integration for reducing energy losses have been reported while considering the time-varying characteristics of both demand and generation. The size of wind DG units is addressed using approaches: optimal power flow [8] and genetic algorithm [9]. DG units based on wind and solar PV technologies are located and sized employing a hybrid method of sensitivity analysis and evolutionary programming [10]. Different technologies of renewable DG (i.e., biomass, wind, and solar) are placed and sized using analytical methods [11] and a probabilistic-based planning approach [12], [13]. However, reductions in reactive power loss and voltage deviation were not formulated in the objective function in [8]–[13] and time-varying load models were not considered in these works as well.

Recently, few studies [6], [7], [14] indicated that the voltage-dependent load models considerably affect the DG penetration planning when compared with the constant load model. However, such works assumed that DG units are dispatchable and allocated at the peak load demand. Although a research [15] indicated the effect of time-varying load models on energy loss assessment in a distribution system with wind DG, the optimal location and size were not addressed. A study [16] reported that time-varying load models have a critical impact on the location and size of DG, but nondispatchable renewable DG with probabilistic generation was not reported in this work.

The review of relevant literatures shows that renewable DG planning that considers probabilistic generation and time-varying load models has not been reported. The contribution of this paper is to study the penetration of PV unit in a distribution system with several different types of time-varying load models. Here, a new IMO-based analytical expression is proposed to identify the size of PV-based DG with an objective of simultaneously reducing active and reactive power losses and voltage deviation. This expression is then adapted to place PV while considering the characteristics of varying time load models and probabilistic generation. Three different types of customers with dissimilar load patterns (i.e., industrial, residential and commercial) and a mix of all these customers are defined by time-varying voltage-dependent load models.

The remainder of this paper is organized as follows. Section II describes load and PV modeling. Section III presents impact indices related to active and reactive power losses, voltage

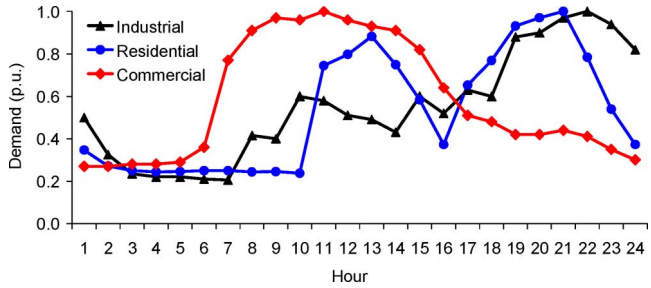

Fig. 1. Normalized daily demand curve for various customers.

TABLE I
LOAD TYPES AND EXPONENTS FOR VOLTAGE-DEPENDENT LOADS

Load types	n_p	n_q
Constant	0	0
Industrial	0.18	6.00
Residential	0.92	4.04
Commercial	1.51	3.40

deviation, and the IMO. An IMO-based analytical approach to accommodate DG unit is also explained in Section IV. Section V presents numerical results and discussions obtained on 69- and 33-bus test distribution systems. Finally, the major contributions and conclusions of the work are summarized in Section VI.

II. LOAD AND SOLAR PV MODELING

A. Load Modeling

The demand of the system considered in this paper is assumed to follow different normalized daily load patterns (i.e., industrial, residential, and commercial) with a peak of 1 p.u., as shown in Fig. 1 [17]. For each load model, the load factor (LF) or the *average load level* of the system can be defined as the area under the load curve in p.u. divided by the total duration [11]

$$\mathrm{LF} = \sum_{t=1}^{24} \frac{p.u.\,demand(t)}{24}. \tag{1}$$

The time-varying voltage-dependent load model or the time-varying load model is defined as a load model which is dependent on the time and voltage. Accordingly, the voltage dependent load model in [18] which incorporates time-varying loads at period t can be expressed as follows:

$$P_k(t) = P_{ok}(t) \times V_k^{n_p}(t) \qquad Q_k(t) = Q_{ok}(t) \times V_k^{n_q}(t) \tag{2}$$

where P_k and Q_k are, respectively, the active and reactive power injections at bus k, P_{ok} and Q_{ok} are, respectively, the active and reactive load at bus k at nominal voltage, V_k is the voltage at bus k, and n_p and n_q are, respectively, the active and reactive load voltage exponents as given in Table I [18].

B. Solar PV Modeling

1) Solar Irradiance Modeling: The solar irradiance for each hour of the day is modeled by the Beta probability density function (PDF) based on historical data which have been collected for three years. To obtain this PDF, a day is split into 24-h periods (time segments), each of which is one hour and has its own solar irradiance PDF. From the collected historical data, the mean and standard deviation of the hourly solar irradiance of the day is calculated. It is assumed that each hour has 20 states for solar irradiance with a step of 0.05 kW/m^2. From the calculated mean and standard deviation, the PDF with 20 states for solar irradiance is generated for each hour of the day, and the probability of each solar irradiance state is determined. Accordingly, the PV output power is obtained for that hour. The model is explained below.

The probabilistic nature of solar irradiance can be described using the PDF reported [19]. This model has been employed in many PV studies such as [10], [12], [20], [21]. Over each period (1 h in this study), the PDF for solar irradiance s can be expressed as follows:

$$f_b(s) = \begin{cases} \frac{\Gamma(\alpha+\beta)}{\Gamma(\alpha)\Gamma(\beta)} s^{(\alpha-1)}(1-s)^{(\beta-1)}, & 0 \le s \le 1,\ \alpha,\ \beta \ge 0 \\ 0, & \text{otherwise} \end{cases} \tag{3}$$

where $f_b(s)$ is the Beta distribution function of s, s is the random variable of solar irradiance (kW/m^2), α and β are parameters of $f_b(s)$, which are calculated using the mean (μ) and standard deviation (σ) of solar irradiance s as follows:

$$\beta = (1-\mu)\left(\frac{\mu(1+\mu)}{\sigma^2} - 1\right) \qquad \alpha = \frac{\mu \times \beta}{1-\mu}.$$

The probability of the solar irradiance state s during any specific hour can be calculated from (3) as follows [12]:

$$\rho(s) = \int_{s1}^{s2} f_b(s)ds \tag{4}$$

where s_1 and s_2 are solar irradiance limits of state s.

The output power from the PV module at solar irradiance s, $P_{PV_o}(s)$ can be expressed as [10], [12], [20]

$$P_{PV_o}(s) = N \times FF \times V_y \times I_y \tag{5}$$

where

$$\begin{aligned} \mathrm{FF} &= \frac{V_{MPP} \times I_{MPP}}{V_{oc} \times I_{sc}} \\ V_y &= V_{oc} - K_v \times T_{cy} \\ I_y &= s\,[I_{sc} + K_i \times (T_{cy} - 25)] \\ T_{cy} &= T_A + s\left(\frac{N_{OT} - 20}{0.8}\right). \end{aligned}$$

Here, N are the number of modules, T_{cy} and T_A are, respectively, cell and ambient temperatures (°C), K_i and K_v are, respectively, current and voltage temperature coefficients (A/°C and V/°C), N_{OT} is nominal operating temperature of cell in °C, FF is fill factor, V_{oc} and I_{sc} are, respectively, the open-circuit voltage (V) and short-circuit current (A), and V_{MPP} and I_{MPP} are, respectively, the voltage and current at maximum power point.

The total expected output power (average output power) of a PV module across any specific period t, $P_{\mathrm{PV}}(t)$ (t = 1 h), can be obtained from (4) and (5) as follows [12]:

$$P_{\mathrm{PV}}(t) = \int_0^1 P_{\mathrm{PV}_o}(s)\rho(s)ds. \tag{6}$$

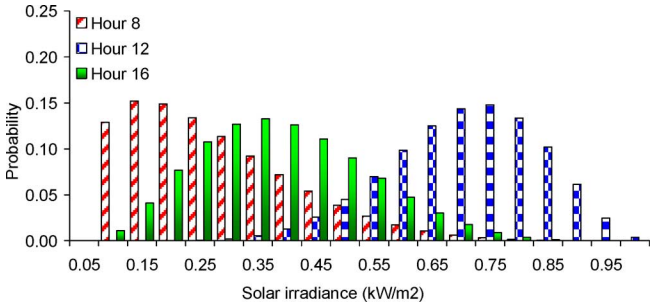

Fig. 2. PDF for solar irradiance at hours 8, 12, and 16.

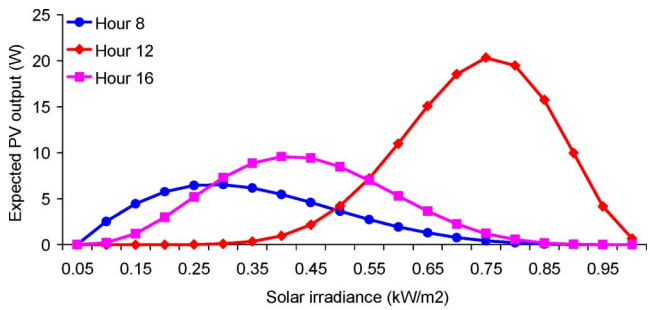

Fig. 3. Expected output of a PV module at hours 8, 12, and 16.

For example, given the mean (μ) and standard deviation (σ) of the hourly solar irradiance found in the Appendix (cf. Table IV), the PDF for 20 solar irradiance states with an interval of 0.05 kW/m^2 for periods 8, 12, and 16 are generated using (3)–(4) and plotted in Fig. 2. Obviously, as the solar irradiance is time- and weather-dependent, different periods have different PDFs. The area under the curve of each hour is unity. Another example is that, given the parameters of a PV module found in the Appendix (cf. Table V), the expected output of the PV module with respect to 20 solar irradiance states (Fig. 2) is calculated using (6) and plotted in Fig. 3. For period 8, the total expected output power, which is calculated as the area under the curve of that period (Fig. 3), is 53.08 W. As the period is assumed at one hour, the PV module is expected to output at 53.08 Wh. Similarly, the expected PV outputs for periods 12 and 16 are found to be 129.96 and 73.42 Wh, respectively. It is observed from Fig. 3 that a difference in the expected PV output patterns exists among hours 8, 12, and 16.

2) Capacity Factor: The capacity factor of a PV module ($\mathrm{CF_{PV}}$) can be defined as the average output power ($P_{\mathrm{PV}}^{\mathrm{avg}}$) divided by the rated power or maximum output ($P_{\mathrm{PV}}^{\mathrm{max}}$) [12]:

$$\mathrm{CF_{PV}} = \frac{P_{\mathrm{PV}}^{\mathrm{avg}}}{P_{\mathrm{PV}}^{\mathrm{max}}}. \tag{7}$$

Once the average output power is calculated using (6) for each hour based on three years of the collected historical data as previously mentioned, the average and maximum output power values are obtained for the day. The $\mathrm{CF_{PV}}$ is then obtained using (7).

3) PV Penetration Level: is the ratio of the total amount of PV energy exported to a network and its total energy consumption [11].

4) PV Generation Criteria: Under the recommendation of the current standard IEEE 1547, PV inverters are not permitted to generate reactive power to the grid [22]. Consequently, the inadequacy of reactive power support for voltage regulation may exist in distribution systems, given a high PV penetration with active power injection only. Conventional devices such as switchable capacitors, voltage regulators, and tap changers are actually utilized for automatic voltage regulation, but they are not sufficiently fast to compensate for transient events due to the PV intermittency [23]. It is likely that the shortage of reactive power support may be an immediate concern at the distribution system level in the future. On the other hand, depending on time and weather variability, the simultaneous occurrence of excess PV generation and low demand would lead to loss of voltage regulation along with unexpected voltage rise on the feeders due to reverse power flows [24]. As a fast response device, the inverter-based PV unit is allowed to inject or absorb reactive power to stabilize load voltages as per the new German grid code [25], while supplying energy as a primary purpose. Therefore, the inverter-based PV technology [23], [26], which is capable of delivering active power and exporting or consuming reactive power, is adopted in this study. The relationship between the active and reactive power of a PV unit at bus k (P_{PV_k} and Q_{PV_k}) is expressed as [27]

$$Q_{\mathrm{PV}_k} = a_k P_{\mathrm{PV}_k} \tag{8}$$

where $a_k = \pm \tan\left(\cos^{-1}\left(pf_{\mathrm{PV}_k}\right)\right)$, a_k is positive for the PV unit supplying reactive power and negative for the PV unit consuming reactive power, and pf_{PV_k} is the operating power factor of the PV unit at bus k.

C. Combined Generation-Load Model

To incorporate the PV output powers as multistate variables in the problem formulation, the combined generation-load model reported in [12] is adopted in this study. The continuous PDF has been split into different states. As previously mentioned, each day has 24-h periods (time segments), each of which has 20 states for solar irradiance with a step of 0.05 kW/m^2 for calculating the PV output powers. As the load demand is constant during each hour, its probability is unity. Therefore, the probability of any combination of the generation and load is the probability of the generation itself.

III. Problem Formulation

A. Impact Indices

Three typical indices employed to describe PV impacts on the distribution system are defined as follows.

1) Active Power Loss Index: Fig. 4(a) shows an n-branch radial distribution system without PV unit, where P_i and Q_i are, respectively, the active and reactive power flow through branch i, and P_{Di} and Q_{Di} are the active and reactive load powers, respectively, at bus i. Fig. 4(b) presents this system with a PV unit located at any bus, say bus k, where P_{PV_k} and Q_{PV_k} are the active and reactive powers, respectively, of the PV unit at bus k. In this case, bus k is identical to bus $i+1$. As shown

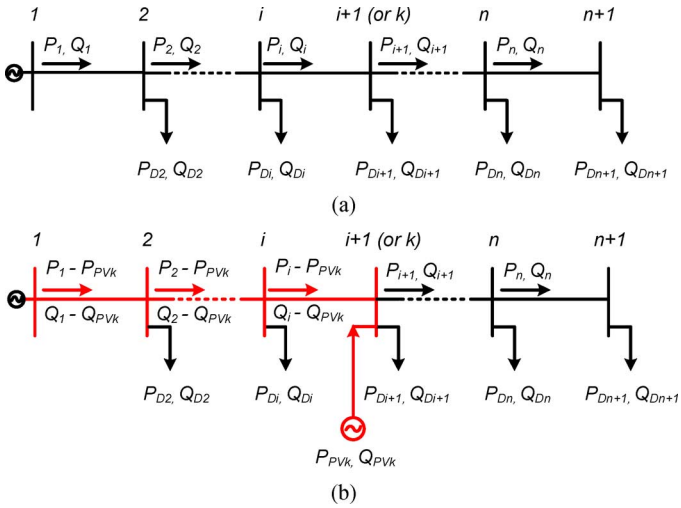

Fig. 4. Radial distribution system: (a) without PV and (b) with PV.

in Fig. 4(a), the total active power loss in the n-branch system without PV (P_L) can be written as [28]

$$P_L = \sum_{i=1}^{n} \frac{P_i^2 + Q_i^2}{|V_i|^2} R_i \tag{9}$$

where R_i is the resistance of branch i, and $|V_i|$ is the voltage magnitude at bus i. As illustrated in Fig. 4(b), due to the active and reactive powers of PV unit injected at bus k, the active and reactive powers flowing from the source to bus k is reduced, whereas the power flows in the remaining branches are unchanged. Accordingly, the power loss (9) can be rewritten as follows:

$$\begin{aligned} P_{L_{\rm PV}} =& \sum_{i=1}^{k} \frac{(P_i - P_{{\rm PV}_k})^2}{|V_i|^2} R_i + \sum_{i=k+1}^{n} \frac{P_i^2}{|V_i|^2} R_i \\ &+ \sum_{i=1}^{k} \frac{(Q_i - Q_{{\rm PV}_k})^2}{|V_i|^2} R_i + \sum_{i=k+1}^{n} \frac{Q_i^2}{|V_i|^2} R_i. \end{aligned} \tag{10}$$

Substituting (8) and (9) into (10), we obtain:

$$\begin{aligned} P_{L_{PV}} =& \sum_{i=1}^{k} \frac{P_{PV_k}^2 - 2P_i P_{PV_k}}{|V_i|^2} R_i \\ &+ \sum_{i=1}^{k} \frac{a_k^2 P_{PV_k}^2 - 2Q_i a_k P_{PV_k}}{|V_i|^2} R_i + P_L. \end{aligned} \tag{11}$$

Finally, the active power loss index (*ILP*) can be defined as the ratio of (11) and (9) as:

$$ILP = \frac{P_{L_{PV}}}{P_L}. \tag{12}$$

2) Reactive Power Loss Index: The total reactive power loss (Q_L) in a radial distribution system with n branches can be written as

$$Q_L = \sum_{i=1}^{n} \frac{P_i^2 + Q_i^2}{|V_i|^2} X_i \tag{13}$$

where X_i is the reactance of branch i. Similar to (11), when both $P_{{\rm PV}_k}$ and $Q_{{\rm PV}_k} = a_k P_{{\rm PV}_k}$ are injected at bus k, (13) can be rewritten as

$$\begin{aligned} Q_{L_{\rm PV}} =& \sum_{i=1}^{k} \frac{P_{{\rm PV}_k}^2 - 2P_i P_{{\rm PV}_k}}{|V_i|^2} X_i \\ &+ \sum_{i=1}^{k} \frac{a_k^2 P_{{\rm PV}_k}^2 - 2Q_i a_k P_{{\rm PV}_k}}{|V_i|^2} X_i + Q_L. \end{aligned} \tag{14}$$

Finally, the reactive power loss index (ILQ) can be defined as the ratio of (14) and (13) as

$${\rm ILQ} = \frac{Q_{L_{\rm PV}}}{Q_L}. \tag{15}$$

3) Voltage Deviation Index: As shown in Fig. 4(a), the voltage deviation (VD) along the branch from bus i to bus $i+1$, $(R_i + jX_i)$, can be expressed as [29]

$$|{\rm VD}_i| = \frac{|R_i P_i + X_i Q_i|}{|V_{i+1}|}. \tag{16}$$

From (16), the total voltage deviation squared (VD^2) in the whole system with n branches can be written as

$$VD^2 = \sum_{i=1}^{n} \frac{(R_i P_i + X_i Q_i)^2}{|V_{i+1}|^2}. \tag{17}$$

When both $P_{{\rm PV}_k}$ and $Q_{{\rm PV}_k}$ are injected at bus k [Fig. 4(b)], (17) can be rewritten as

$$\begin{aligned} {\rm VD}_{\rm PV}^2 =& \sum_{i=1}^{k} \frac{R_i^2 (P_i - P_{{\rm PV}_k})^2}{|V_{i+1}|^2} + \sum_{i=k+1}^{n} \frac{R_i^2 P_i^2}{|V_{i+1}|^2} \\ &+ \sum_{i=1}^{k} \frac{X_i^2 (Q_i - Q_{{\rm PV}_k})^2}{|V_{i+1}|^2} + \sum_{i=k+1}^{n} \frac{X_i^2 Q_i^2}{|V_{i+1}|^2} \\ &+ 2 \sum_{i=1}^{k} \frac{R_i X_i (P_i - P_{{\rm PV}_k})(Q_i - Q_{{\rm PV}_k})}{|V_{i+1}|^2} \\ &+ 2 \sum_{i=k+1}^{n} \frac{R_i X_i P_i Q_i}{|V_{i+1}|^2}. \end{aligned} \tag{18}$$

Substituting (8) and (17) into (18), we obtain

$$\begin{aligned} {\rm VD}_{\rm PV}^2 =& \sum_{i=1}^{k} \frac{R_i^2 \left(P_{{\rm PV}_k}^2 - 2P_i P_{{\rm PV}_k}\right)}{|V_{i+1}|^2} \\ &+ \sum_{i=1}^{k} \frac{X_i^2 \left(a_k^2 P_{{\rm PV}_k}^2 - 2Q_i a_k P_{{\rm PV}_k}\right)}{|V_{i+1}|^2} \\ &- 2 \sum_{i=1}^{k} \frac{R_i X_i \left(P_i a_k P_{{\rm PV}_k} + Q_i P_{{\rm PV}_k} - a_k P_{{\rm PV}_k}^2\right)}{|V_{i+1}|^2} \\ &+ {\rm VD}^2. \end{aligned} \tag{19}$$

Finally, the voltage deviation index (IVD) of a distribution system can be defined as the ratio of (19) and (17) as follows:

$${\rm IVD} = \frac{{\rm VD}_{\rm PV}^2}{{\rm VD}^2}. \tag{20}$$

B. Multiobjective Index

On the one hand, when PV unit is allocated for minimizing either the active or reactive power loss (i.e., ILP or ILQ, respectively), this would potentially limit the PV penetration with a high voltage deviation. On the other hand, a high penetration could be achieved when PV unit is considered for reducing the voltage deviation (IVD) alone, but the system losses could be high. To include all the indices in the analysis, a multiobjective index (IMO) can be defined as a combination of the ILP, ILQ, and IVD indices with proper weights as follows:

$$\mathrm{IMO} = \sigma_1 \mathrm{ILP} + \sigma_2 \mathrm{ILQ} + \sigma_3 \mathrm{IVD} \tag{21}$$

where $\sum_{i=1}^{3} \sigma_i = 1.0$ and $\sigma_i \in [0, 1]$, $i = 1, 2, 3$.

This can be performed as all impact indices are normalized with values between zero and one [6]. When PV unit is not connected to the system (i.e., base case system), the IMO is the highest at one.

The weights are intended to give the relative importance to each impact index for PV allocation and depend on the analysis purpose (e.g., planning or operation) [5]–[7], [30]. The determination of proper values for the weighting factors will also depend on the experience and concerns of the system planner. The PV installation has a significant impact on the active and reactive power losses and voltage profiles. The active power loss is currently one of the major concerns due to its impact on the distribution utilities' profit, while the reactive power loss and voltage profile are less important than the active power loss. Considering these concerns and referring to previous reports in [5]–[7], [30], this study assumes that the active power loss receives a significant weight of 0.5, leaving the reactive power loss and the voltage deviation of 0.25 each. However, the above weights can be adjusted based on the priority.

As the solar irradiance is a random variable, the PV output power and its corresponding IMO as defined by (21) are stochastic during each hour. The IMO can be formulated in the expected value. To calculate the IMO, the power load flow is analyzed for each combined generation-load state. It is assumed that $\mathrm{IMO}(s)$ is the expected IMO at solar irradiance s, the total expected IMO over any specific period t, $\mathrm{IMO}(t)$ ($t =$ 1 h) can be formulated as a combination of (4) and (21) as follows:

$$\mathrm{IMO}(t) = \int_0^1 \mathrm{IMO}(s)\rho(s)ds. \tag{22}$$

The average IMO (AIMO) over the total period ($T = 24$) in a system with PV unit can be obtained from (22) as

$$\mathrm{AIMO} = \frac{1}{T}\int_0^T \mathrm{IMO}(t)dt = \frac{1}{T}\sum_{t=1}^{T} \mathrm{IMO}(t) \times \Delta t \tag{23}$$

where Δt is the time duration or time segment of period t (one hour in this study). The lowest AIMO implies the best PV allocation for reducing active and reactive power losses and enhancing voltage profiles.

IV. Proposed Analytical Approach

A. Sizing PV

Most of the existing analytical methods address DG allocation only for the reduction of real power loss as a single-objective function [11], [27], [31]–[33]. This paper proposes a new analytical expression based on the IMO as given by (21) for sizing PV-based DG at a pre-defined power factor. Substituting (12), (15), and (20) into (21), we get

$$\mathrm{IMO} = \frac{\sigma_1}{P_L}P_{\mathrm{LPV}} + \frac{\sigma_2}{Q_L}Q_{\mathrm{LPV}} + \frac{\sigma_3}{\mathrm{VD}^2}\mathrm{VD}_{\mathrm{PV}}^2. \tag{24}$$

To find the minimum IMO value, the partial derivative of (24) with respect to P_{PV_k} becomes zero, shown as follows:

$$\frac{\partial \mathrm{IMO}}{\partial P_{\mathrm{PV}_k}} = \frac{\sigma_1}{P_L}\frac{\partial P_{\mathrm{LPV}}}{\partial P_{\mathrm{PV}_k}} + \frac{\sigma_2}{Q_L}\frac{\partial Q_{\mathrm{LPV}}}{\partial P_{\mathrm{PV}_k}} + \frac{\sigma_3}{\mathrm{VD}^2}\frac{\partial \mathrm{VD}_{\mathrm{PV}}^2}{\partial P_{\mathrm{PV}_k}} = 0. \tag{25}$$

The partial derivatives of (11), (14), and (19) with respect to P_{PV_k} can be written as

$$\frac{\partial P_{\mathrm{LPV}}}{\partial P_{\mathrm{PV}_k}} = -2A_k + 2C_k P_{\mathrm{PV}_k} - 2B_k a_k + 2C_k a_k^2 P_{\mathrm{PV}_k} \tag{26}$$

$$\frac{\partial Q_{\mathrm{LPV}}}{\partial P_{\mathrm{PV}_k}} = -2D_k + 2F_k P_{\mathrm{PV}_k} - 2E_k a_k + 2F_k a_k^2 P_{\mathrm{PV}_k} \tag{27}$$

$$\begin{aligned}\frac{\partial \mathrm{VD}_{\mathrm{PV}}^2}{\partial P_{\mathrm{PV}_k}} =& 2G_k P_{\mathrm{PV}_k} - 2H_k + 2I_k a_k^2 P_{\mathrm{PV}_k} - 2J_k a_k \\ & - 2K_k a_k - 2L_k + 4M_k a_k P_{\mathrm{PV}_k}\end{aligned} \tag{28}$$

where

$$A_k = \sum_{i=1}^{k}\frac{R_i P_i}{|V_i|^2} \quad B_k = \sum_{i=1}^{k}\frac{R_i Q_i}{|V_i|^2} \quad C_k = \sum_{i=1}^{k}\frac{R_i}{|V_i|^2}$$

$$D_k = \sum_{i=1}^{k}\frac{X_i P_i}{|V_i|^2} \quad E_k = \sum_{i=1}^{k}\frac{X_i Q_i}{|V_i|^2} \quad F_k = \sum_{i=1}^{k}\frac{X_i}{|V_i|^2}$$

$$G_k = \sum_{i=1}^{k}\frac{R_i^2}{|V_{i+1}|^2} \quad H_k = \sum_{i=1}^{k}\frac{R_i^2 P_i}{|V_{i+1}|^2} \quad I_k = \sum_{i=1}^{k}\frac{X_i^2}{|V_{i+1}|^2}$$

$$J_k = \sum_{i=1}^{k}\frac{X_i^2 Q_i}{|V_{i+1}|^2}$$

$$K_k = \sum_{i=1}^{k}\frac{R_i X_i P_i}{|V_{i+1}|^2} \quad L_k = \sum_{i=1}^{k}\frac{R_i X_i Q_i}{|V_{i+1}|^2} \quad M_k = \sum_{i=1}^{k}\frac{R_i X_i}{|V_{i+1}|^2}.$$

Substituting (26)–(28) into (25), we obtain

$$P_{\mathrm{PV}_k} = \frac{\left[\begin{array}{l}\frac{\sigma_1}{P_L}\left(A_k + a_k B_k\right) + \frac{\sigma_2}{Q_L}\left(D_k + a_k E_k\right) \\ + \frac{\sigma_3}{\mathrm{VD}^2}\left(H_k + a_k J_k + a_k K_k + L_k\right)\end{array}\right]}{\left[\begin{array}{l}\frac{\sigma_1}{P_L}\left(C_k + a_k^2 C_k\right) + \frac{\sigma_2}{Q_L}\left(F_k + a_k^2 F_k\right) \\ + \frac{\sigma_3}{\mathrm{VD}^2}\left(G_k + a_k^2 I_k + 2a_k M_k\right)\end{array}\right]}. \tag{29}$$

The power factor of PV depends on the operating conditions and technology adopted. Given a pf_{PV_k} or a_k value, the active

power size of PV for the minimum IMO can be obtained from (29). The reactive power size is then obtained using (8).

B. Computational Procedure

Here, a computational procedure is developed to allocate PV unit for reducing the AIMO while considering the time-varying load models and probabilistic generation. To reduce the computational burden, the IMO is first minimized at the average load level as defined by (1) to specify the location of PV unit. This average load level has a significantly larger duration than other loading levels (e.g., peak or low load levels). The size is then calculated at that location based on the probabilistic PV output curve by minimizing the AIMO over all periods as given by (23). The computational procedure is summarized in the following steps.

Step 1) Run load flow for the system without PV unit at the average load level or at the system load factor (LF) using (1) and calculate the IMO using (21).

Step 2) Specify the location and size at a pre-defined power factor of PV unit at the average load level only.
   a) Find the PV size at each bus ($P^{\text{avg}}_{\text{PV}_k}$) using (29).
   b) Place PV unit obtained earlier at each bus and calculate the IMO for each case using (21).
   c) Locate the optimal bus at which the IMO is minimum with the corresponding size of PV unit at the average load level ($P^{\text{avg}}_{\text{PV}_k}$) at that bus.

Step 3) Find the capacity factor of PV unit ($CF_{\text{PV}k}$) using (7).

Step 4) Find the optimal size of PV unit i.e., its maximum output ($P^{\text{max}}_{\text{PV}_k}$), at the optimal location obtained in *Step* 2 as follows, where depending on the patterns of demand and generation, an adjusted factor, k_{PV} (e.g., 0.8, 0.9, or 1.1) could be used to achieve a better outcome:

$$P^{\text{max}}_{\text{PV}_k} = k_{\text{PV}} \times \frac{P^{\text{avg}}_{\text{PV}_k}}{\text{CF}_{\text{PV}_k}}. \tag{30}$$

Step 5) Find the PV output at the optimal location for period t as follows, where $\text{p.u.}\,\text{PV}\,\text{output(t)}$ is the PV output in p.u. at period t, which is calculated using (3)–(6) and normalized:

$$P_{\text{PV}k}(t) = p.u.\,\text{PV}\ output(t) \times P^{\text{max}}_{\text{PV}k}. \tag{31}$$

Step 6) Run load flow with each PV output obtained in step 5) for each state over all of the periods of the day and calculate the AIMO using (23).

Step 7) Repeat steps 4)–6) by adjusting k_{PV} in (30) until the minimum AIMO is obtained.

The above computational procedure was developed to place a single PV unit. However, it can be easily modified to accommodate multiple PV units by adding an iterative algorithm as reported in our study [34].

V. Case Study

A. Test Systems

The proposed approach has been applied to two radial test distribution systems. The first system in Fig. 5 has 69 buses and a peak demand of 3800 kW and 2690 kVAr [35]. The second system in Fig. 6 has 33 buses and a peak demand of 3715 kW and 2300 kVAr [36]. The constraint of operating voltages is assumed from 0.95 to 1.05 p.u. [22]. The proposed approach has been simulated in MATLAB environment.

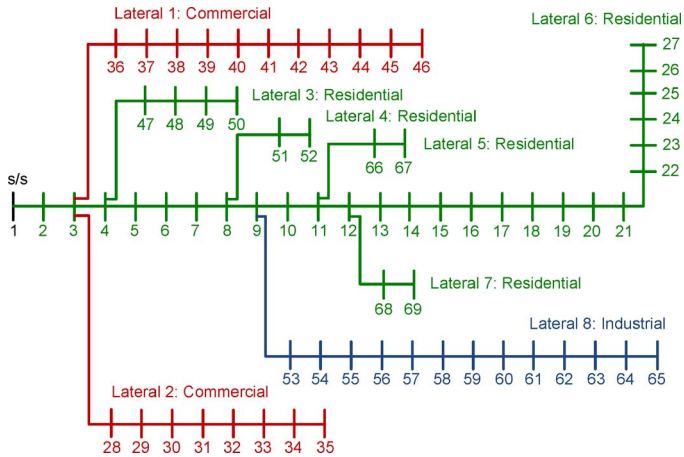

Fig. 5. The 69-bus test distribution system.

1) Load Modeling: Five types of time-varying load models are considered in this study:

1) time-varying industrial load model;
2) time-varying residential load model;
3) time-varying commercial load model;
4) time-varying mixed load model;
5) time-varying constant load model.

For both test systems, these loads are modeled by (2) by combining the time-varying demand patterns for industrial, residential, and commercial loads in Fig. 1 with the voltage-dependent load type with appropriate voltage exponents defined in Table I.

2) Solar PV Modeling: The presented method can be applied to either solar farm or roof-top PV. However, the roof-top PV has been considered as an example to validate the proposed methodology in this paper. It is assumed that PV unit provides active and reactive power at a lagging power factor of 0.9 which is compliant with the new German grid code [25]. The mean and standard deviation (i.e., μ and σ, respectively) for each hour of a day are calculated using the hourly historical solar irradiance data collected for three years, as provided in Appendix (Table IV).[1] The characteristics of a PV module [20] employed for the PV model (5) are also found in the Appendix (Table V). The solar irradiance s is considered at an interval of 0.05 kW/m^2. Using (3)–(6), the hourly expected output of the PV module is calculated and plotted in Fig. 7(a)–(c). It is observed from these figures that a difference in the PV output patterns exists among hours 6–19. Actually, this is due to dependence of the PV output on the solar irradiance, ambient temperature and the characteristics of the PV module itself. The total expected output power for each hour can be calculated as a summation of all the expected output powers at that hour. Accordingly, the normalized expected PV output for the 24-h period day is plotted in Fig. 8.

[1][Online]. Available: https://solaranywhere.com/

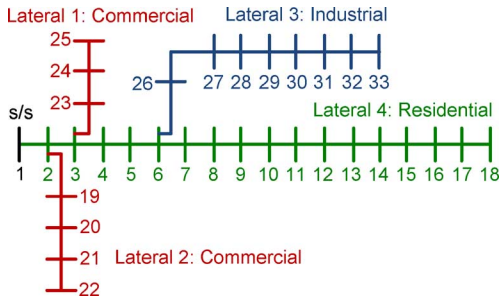

Fig. 6. The 33-bus test distribution system.

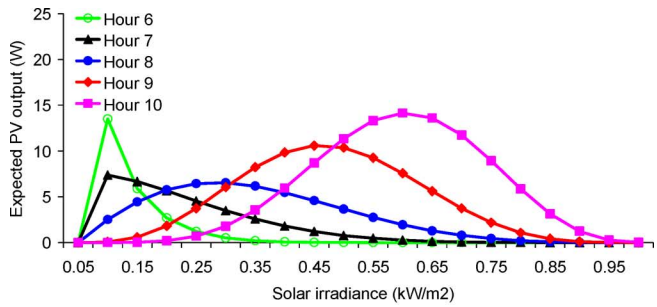

(a)

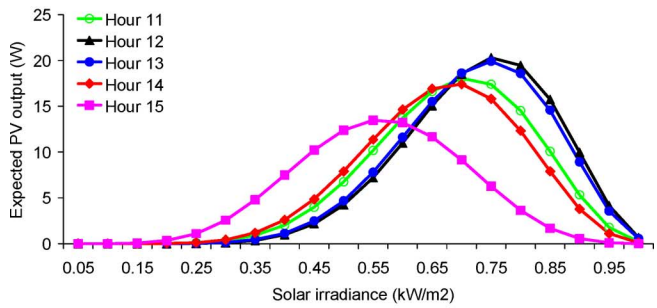

(b)

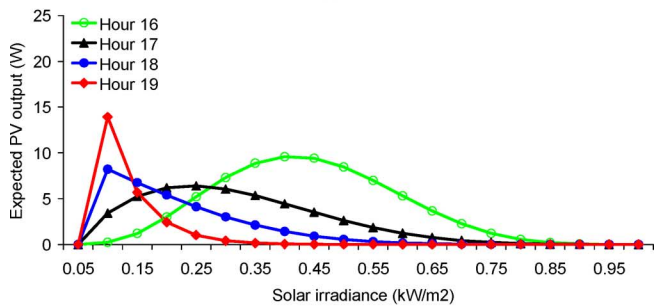

(c)

Fig. 7. Expected PV output for hours: (a) 6–10, (b) 11–15, and (c) 16–19.

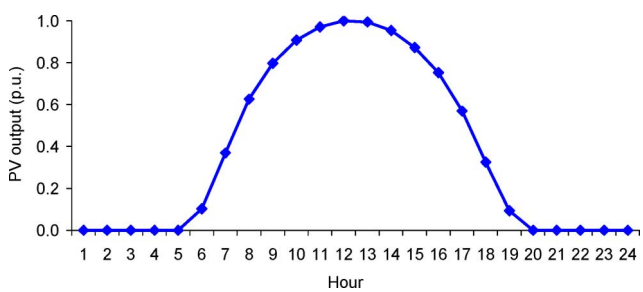

Fig. 8. Normalized daily expected PV output.

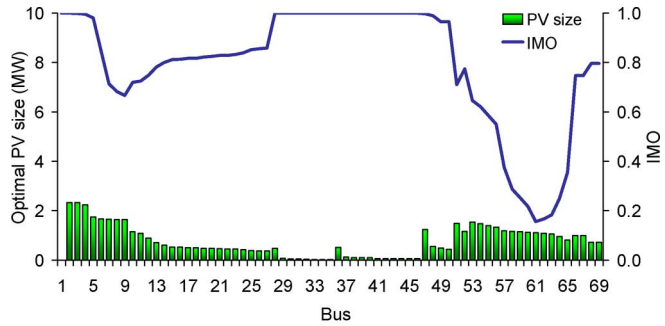

(a)

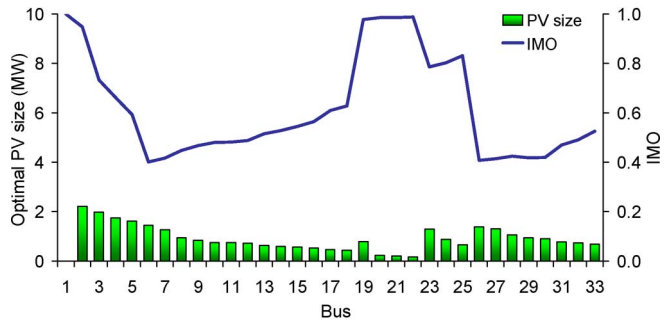

(b)

Fig. 9. PV size with respect to IMO at various locations at average load level for the industrial load model: (a) 69-bus system and (b) 33-bus system.

B. Location Selection

As previously mentioned, to select the best location, PV unit is sized at various buses using (29) after running one base case load flow at average load level and the corresponding multi-objective (IMO) for each bus is calculated. The best location at which the lowest IMO is subsequently determined. Fig. 9(a) shows the optimal sizes of PV unit at various buses with the corresponding IMO values in the 69-bus system with the industrial load model. The sizes are significantly different in the range of 0.39 to 2.34 MW. It is observed from the figure that the best location is bus 61 where the IMO is minimum. Similarly, the best location is specified at bus 6 in the 33-bus system with the industrial load model, as depicted in Fig. 9(b). It is noticed that given a fixed location due to resource availability and geographic limitations, the optimal size to which the IMO is minimum can be identified from the respective figures. For the other load models (i.e., constant, residential, commercial and mixed), the best locations are at buses 61 and 6 in the 69- and 33-bus systems, respectively. However, depending on the daily demand patterns and characteristic of systems, the locations may be different among load models.

C. Sizing With Respect to Indices

For the 69-bus system, Fig. 10 shows the hourly expected outputs of the PV unit at bus 61 over one day (06:00 to 19:00) with different time-varying load models. These PV output patterns exactly follow the expected PV output curve depicted in Fig. 8. The maximum output of the PV unit for each load models, which is indentified at hour 11, shows its optimum size. Fig. 11 presents the expected IMO values which are respectively obtained for the 69-bus system with the PV unit. At each period of

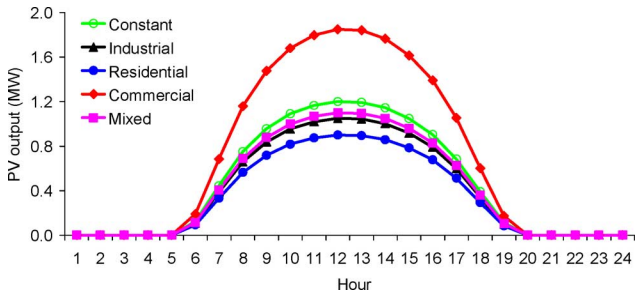

Fig. 10. Hourly expected PV outputs at bus 61 for the 69-bus system for different time-varying load models.

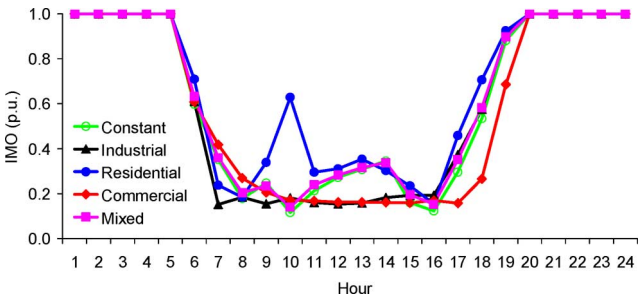

Fig. 11. Hourly expected IMO curves for the 69-bus system with a PV at bus 61 for different time-varying load models.

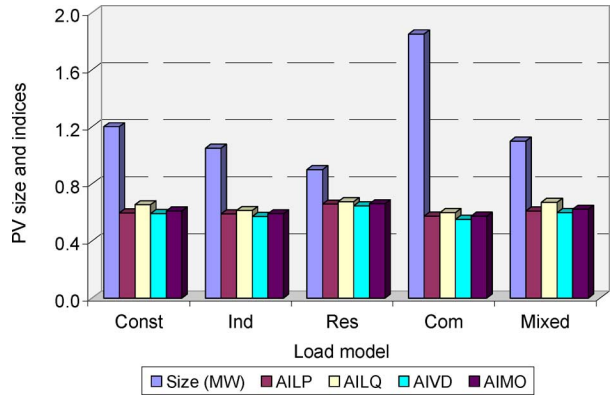

Fig. 12. PV size and indices for the 69-bus system with PV at bus 61 for different time-varying load models.

TABLE II
PV ALLOCATION IN THE 69- AND 33-BUS SYSTEMS

Load models	69-bus System			33-bus system		
	Bus	Size (MW)	AIMO	Bus	Size (MW)	AIMO
Const	61	1.20	0.609	6	1.80	0.737
Ind	61	1.05	0.590	6	1.55	0.722
Res	61	0.90	0.660	6	1.15	0.770
Com	61	1.85	0.573	6	2.50	0.716
Mixed	61	1.10	0.622	6	1.65	0.754

the day, the IMO values in the system with PV unit are substantially declined when compared to the system without PV unit (IMO $=$ 1 p.u.). This indicates that the PV installation positively affects the IMO. Fig. 12 shows a comparison of the optimal PV size, and the averages of IMO and its components (ILP, ILQ, and IVD) in the 69-bus system for different time-varying load models. As shown in Fig. 12, a significant difference in the optimal size of PV is observed when different time-varying load models are considered. The PV size for the commercial load is remarkably larger than the industrial and residential loads. This is due to the fact that the commercial consumption and PV output availability (Figs. 1 and 10) almost occurred simultaneously during the day, while the industrial and residential customers had most of the consumption during the night. It is revealed from Fig. 12 that the maximum PV size is determined for the commercial load, whereas the minimum value is identified for the residential load. In addition, the size of the PV unit for the time-varying constant load model is roughly 9.09% bigger than the time-varying mixed load model. A similar trend has been observed for the 33-bus system.

Table II shows a summary and comparison of the results of PV allocation obtained in the 69- and 33-bus systems with different time-varying load models. The results include the optimum bus, size and penetration of the PV unit and corresponding AIMO for each load model. Differences in the location, size and penetration exist among the load models. For the 69-bus system, the minimum and maximum AIMO values are respectively 0.573 p.u. for the commercial load model and 0.660 p.u. for the residential load model. A similar trend is observed for the 33-bus system. The lowest AIMO is 0.716 p.u. for the commercial load model, while the highest AIMO is 0.770 p.u. for the residential load model.

D. PV Penetration and Energy Losses

Fig. 13 shows the PV penetration levels in the 69- and 33-bus systems with different time-varying load models. First, it is observed that the time-varying load models adopted have a diverse impact on the penetration level. In the 69-bus system, the penetrations are 32.59% for the commercial load model and 19.55% and 17.38% for the industrial and residential load models, respectively. This is because the PV generation pattern (Fig. 8) matches better with the commercial demand than the industrial and residential demand curves (Fig. 1). Similarly, in the 33-bus system, the penetration levels are 45.23% for the commercial load model and 29.64% and 22.80% for the industrial and residential load models, respectively. Second, it is observed from Fig. 13 that there is a difference in the PV penetration between the time-varying constant and mixed load models in both test systems. In the 69-bus system, the PV penetration is 22.18% for the time-varying constant load model, while this value is 20.34% for the time-varying mixed load model. Similarly, in the 33-bus system, the PV penetrations are 34.18% and 31.33% for the time-varying constant and mixed load models, respectively. Finally, it is also observed that the system load characteristics play a crucial role in determining the PV penetration. For each load model, the PV penetration in the 69-bus system is lower than the 33-bus system, as shown in Fig. 13.

Table III shows a summary and comparison of the energy loss of the system without and with PV unit over a day (E_L and E_{LPV}, respectively) for different time-varying load models. The daily energy loss is calculated as a sum of all hourly power losses over the day. For each load model, it is observed that the energy loss of the system with PV unit is significantly reduced when compared to that of the system without PV. In

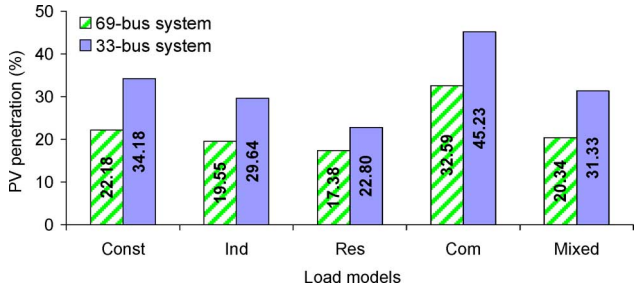

Fig. 13. PV penetration levels in the 69- and 33-bus systems.

TABLE III
ENERGY LOSS REDUCTION OVER A DAY FOR 69- AND 33-BUS SYSTEMS

Load models	69-bus System			33-bus system		
	E_L (MWh)	E_{LPV} (MWh)	ΔE (%)	E_L (MWh)	E_{LPV} (MWh)	ΔE (%)
Const	1.87	1.32	29.54	1.73	1.25	28.13
Ind	1.56	1.11	28.50	1.51	1.18	21.32
Res	1.49	1.01	32.28	1.45	1.11	23.33
Com	1.68	0.52	68.90	1.63	0.81	50.20
Mixed	1.54	1.08	29.79	1.43	1.04	27.58

addition, due to inclusion of the active and reactive load voltage exponents in the mixed load model, the energy losses with and without PV unit for this model are respectively lower than the constant load model. Table III also shows the results of the energy loss reduction of the two systems (ΔE) for all load models. In both systems, the maximum loss reduction is observed in the commercial load, whereas the minimum value is obtained in the industrial customer. This is due to the fact that the PV generation better matches with the commercial load than the industrial customer as previously mentioned.

VI. CONCLUSION

This paper has proposed an analytical approach to determine the penetration of PV unit in a distribution system with different types of time-varying load models. Here, a multi-objective index (IMO) based analytical expression is proposed to identify the size of PV unit, which is capable of supplying active and reactive power, with a multi-objective of simultaneously reducing active and reactive power losses and voltage deviation. The analytical expression is then adapted to accommodate PV unit while considering the time-varying characteristics of demand and generation. The Beta PDF model is used to describe the probabilistic nature of solar irradiance. The results indicate that the time-varying load models play a critical role in determining the PV penetration in any distribution system. For residential load model, a poor match between the generation and demand leads to quite low PV penetrations, roughly 17% and 23% in the 69- and 33-bus systems, respectively. Similarly, for industrial load, due to a mismatch between the generation and demand, the 69- and 33-bus systems can accommodate PV penetrations of approximately 20% and 30%, respectively. In contrast, for a commercial load model, a good match between the demand and generation results in higher penetrations at around 33% and 45% in the respective 69- and 33-bus systems. In addition, a practical load model which is defined as a time-varying mixed load model of residential, industrial and commercial types has been examined. It is observed that the PV penetration in the time-varying mixed load model is lower than the time-varying constant load model.

TABLE IV
MEAN AND STANDARD DEVIATION OF SOLAR IRRADIANCE

Hour	μ (kW/m^2)	σ (kW/m^2)	Hour	μ (kW/m^2)	σ (kW/m^2)
6	0.019	0.035	13	0.648	0.282
7	0.096	0.110	14	0.590	0.265
8	0.222	0.182	15	0.477	0.237
9	0.381	0.217	16	0.338	0.204
10	0.511	0.253	17	0.190	0.163
11	0.610	0.273	18	0.080	0.098
12	0.657	0.284	19	0.017	0.032

TABLE V
CHARACTERISTICS OF THE PV MODULE

PV module characteristics	Value
Nominal cell operating temperature, N_{OT} (^{0}C)	43
Current at maximum power point, I_{MPP} (A)	7.76
Voltage at maximum power point, V_{MPP} (V)	28.36
Short circuit current, I_{sc} (A)	8.38
Open circuit voltage, V_{oc} (V)	36.96
Current temperature coefficients, K_i (A /^{o}C)	0.00545
Voltage temperature coefficients, K_v (V /^{o}C)	0.1278

APPENDIX

The mean and standard deviation (i.e., μ and σ, respectively) for each hour of a day are calculated based on the hourly historical solar irradiance data collected for three years, as shown in Table IV . The characteristics of a PV module employed in the PV model (5) are tabulated in Table V [20].

REFERENCES

[1] *Renewables 2012 Global Status Report*, [Online]. Available: http: www.ren21.net
[2] G. Masson, M. Latour, and D. Biancardi, "Global market outlook for photovoltaics until 2016," European Photovoltaic Industry Association, 2012 [Online]. Available: http:// http://www.epia.org/news
[3] S. Eftekharnejad, V. Vittal, G. T. Heydt, B. Keel, and J. Loehr, "Impact of increased penetration of photovoltaic generation on power systems," *IEEE Trans Power Syst.*, vol. 28, no. 2, pp. 893–901, May 2013.
[4] C. Whitaker, J. Newmiller, M. Ropp, and B. Norris, "Distributed photovoltaic systems design and technology requirements," Sandia National Laboratories, 2008 [Online]. Available: http://www1.eere.energy.gov/solar/sunshot/index.html
[5] L. F. Ochoa, A. Padilha-Feltrin, and G. P. Harrison, "Evaluating distributed generation impacts with a multiobjective index," *IEEE Trans Power Del.*, vol. 21, no. 3, pp. 1452–1458, Jul. 2006.
[6] D. Singh and K. S. Verma, "Multiobjective optimization for DG planning with load models," *IEEE Trans. Power Syst.*, vol. 24, no. 1, pp. 427–436, Jan. 2009.
[7] A. M. El-Zonkoly, "Optimal placement of multi-distributed generation units including different load models using particle swarm optimisation," *IET Gener. Transm. Distrib.*, vol. 5, no. 7, pp. 760–771, Jul. 2011.
[8] L. F. Ochoa and G. P. Harrison, "Minimizing energy losses: Optimal accommodation and smart operation of renewable distributed generation," *IEEE Trans. Power Syst.*, vol. 26, no. 1, pp. 198–205, Feb. 2011.
[9] F. Ugranlı and E. Karatepe, "Optimal wind turbine sizing to minimize energy loss," *Int. J. Electr. Power Energy Syst.*, vol. 53, pp. 656–663, Dec. 2013.
[10] D. K. Khatod, V. Pant, and J. Sharma, "Evolutionary programming based optimal placement of renewable distributed generators," *IEEE Trans. Power Syst.*, vol. 28, no. 2, pp. 683–695, May 2013.

[11] D. Q. Hung, N. Mithulananthan, and R. C. Bansal, "Analytical strategies for renewable distributed generation integration considering energy loss minimization," *Appl. Energy*, vol. 105, pp. 75–85, May 2013.
[12] Y. M. Atwa, E. F. El-Saadany, M. M. A. Salama, and R. Seethapathy, "Optimal renewable resources mix for distribution system energy loss minimization," *IEEE Trans. Power Syst.*, vol. 25, no. 1, pp. 360–370, Feb. 2010.
[13] Y. M. Atwa and E. F. El-Saadany, "Probabilistic approach for optimal allocation of wind-based distributed generation in distribution systems," *IET Renew. Power Gener.*, vol. 5, no. 1, pp. 79–88, Jan. 2011.
[14] D. Singh and R. K. Misra, "Effect of load models in distributed generation planning," *IEEE Trans. Power Syst.*, vol. 22, no. 4, pp. 2204–2212, Nov. 2007.
[15] K. Qian, C. Zhou, M. Allan, and Y. Yuan, "Effect of load models on assessment of energy losses in distributed generation planning," *Int. J. Electr. Power Energy Syst.*, vol. 33, no. 6, pp. 1243–1250, Jul. 2011.
[16] R. Ebrahimi, M. Ehsan, and H. Nouri, "A profit-centric strategy for distributed generation planning considering time varying voltage dependent load demand," *Int. J. Electr Power Energy Syst.*, vol. 44, no. 1, pp. 168–178, Jan. 2013.
[17] E. Lopez, H. Opazo, L. Garcia, and P. Bastard, "Online reconfiguration considering variability demand: Applications to real networks," *IEEE Trans. Power Syst.*, vol. 19, no. 1, pp. 549–553, Feb. 2004.
[18] S. G. Casper, C. O. Nwankpa, R. W. Bradish, H.-D. Chiang, C. Concordia, J. V. Staron, C. W. Taylor, E. Vaahedi, and G. Wu, "Bibliography on load models for power flow and dynamic performance simulation," *IEEE Trans. Power Syst.*, vol. 10, no. 1, pp. 523–538, Feb. 1995.
[19] Z. M. Salameh, B. S. Borowy, and A. R. A. Amin, "Photovoltaic module-site matching based on the capacity factors," *IEEE Trans. Energy Convers.*, vol. 10, no. 2, pp. 326–332, Jun. 1995.
[20] J. J. H. Teng, S. W. Luan, D. J. Lee, and Y. Q. Huang, "Optimal charging/discharging scheduling of battery storage systems for distribution systems interconnected with sizeable PV generation systems," *IEEE Trans. Power Syst.*, vol. 28, no. 2, pp. 1425–1433, May 2013.
[21] F. Miao, V. Vittal, G. T. Heydt, and R. Ayyanar, "Probabilistic power flow studies for transmission systems with photovoltaic generation using cumulants," *IEEE Trans. Power Syst.*, vol. 27, no. 3, pp. 2251–2261, Nov. 2012.
[22] *IEEE Standard for Interconnecting Distributed Resources with Electric Power Systems*, IEEE Std 1547, Aug. 2003.
[23] K. Turitsyn, P. Sulc, S. Backhaus, and M. Chertkov, "Options for control of reactive power by distributed photovoltaic generators," *Proc. IEEE*, vol. 99, no. 6, pp. 1063–1073, Jun. 2011.
[24] M. Thomson and D. G. Infield, "Network power-flow analysis for a high penetration of distributed generation," *IEEE Trans. Power Syst.*, vol. 22, no. 3, pp. 1157–1162, Aug. 2007.
[25] A. Samadi, M. Ghandhari, and L. Söder, "Reactive power dynamic assessment of a PV system in a distribution grid," *Energy Procedia*, vol. 20, pp. 98–107, 2012.
[26] F. L. Albuquerque, A. J. Moraes, G. C. Guimarães, S. M. R. Sanhueza, and A. R. Vaz, "Photovoltaic solar system connected to the electric power grid operating as active power generator and reactive power compensator," *Solar Energy*, vol. 84, no. 7, pp. 1310–1317, Jul. 2010.
[27] D. Q. Hung, N. Mithulananthan, and R. C. Bansal, "Analytical expressions for DG allocation in primary distribution networks," *IEEE Trans. Energy Convers.*, vol. 25, no. 3, pp. 814–820, Sep. 2010.
[28] C. Chung-Fu, "Reconfiguration and capacitor placement for loss reduction of distribution systems by ant colony search algorithm," *IEEE Trans. Power Syst.*, vol. 23, no. 4, pp. 1747–1755, Nov. 2008.
[29] F. A. Viawan and D. Karlsson, "Combined local and remote voltage and reactive power control in the presence of induction machine distributed generation," *IEEE Trans. Power Syst.*, vol. 22, no. 4, pp. 2003–2012, Nov. 2007.
[30] L. F. Ochoa, A. Padilha-Feltrin, and G. P. Harrison, "Evaluating distributed time-varying generation through a multiobjective index," *IEEE Trans. Power Del.*, vol. 23, no. 2, pp. 1132–1138, Apr. 2008.
[31] C. Wang and M. H. Nehrir, "Analytical approaches for optimal placement of distributed generation sources in power systems," *IEEE Trans. Power Syst.*, vol. 19, no. 4, pp. 2068–2076, Nov. 2004.
[32] T. Gözel and M. H. Hocaoglu, "An analytical method for the sizing and siting of distributed generators in radial systems," *Electr. Power Syst. Res.*, vol. 79, no. 6, pp. 912–918, Jun. 2009.
[33] N. Acharya, P. Mahat, and N. Mithulananthan, "An analytical approach for DG allocation in primary distribution network," *Int. J. Elect. Power Energy Syst.*, vol. 28, no. 10, pp. 669–678, Dec. 2006.
[34] D. Q. Hung, N. Mithulananthan, and K. Y. Lee, "Optimal placement of dispatchable and nondispatchable renewable DG units in distribution networks for minimizing energy loss," *Int. J. Electr. Power Energy Syst.*, vol. 55, pp. 179–186, Feb. 2014.
[35] M. E. Baran and F. F. Wu, "Optimal capacitor placement on radial distribution systems," *IEEE Trans. Power Del.*, vol. 4, no. 1, pp. 725–734, Jan. 1989.
[36] M. E. Baran and F. F. Wu, "Network reconfiguration in distribution systems for loss reduction and load balancing," *IEEE Trans. Power Del.*, vol. 4, no. 2, pp. 1401–1407, Apr. 1989.

Duong Quoc Hung (S'11) received the M.Eng. degree in electric power system management from the Asian Institute of Technology, Bangkok, Thailand, in 2008. He is currently working toward the Ph.D. degree at the School of Information Technology and Electrical Engineering, University of Queensland, Brisbane, Australia.

He has ten years of experience as an Electrical Engineer with Southern Power Corporation, Electricity of Vietnam (EVN), Vietnam. His research interests are distribution system analysis and the smart integration of distributed renewable generation and battery energy storage.

Nadarajah Mithulananthan (SM'10) received the Ph.D. degree in electrical and computer engineering from the University of Waterloo, Waterloo, ON, Canada, in 2002, the B.Sc. (Eng.) degree from the University of Peradeniya, Sri Lanka, in 1993, and the M.Eng degree from the Asian Institute of Technology, Bangkok, Thailand, in 1997.

He was an Electrical Engineer with the Generation Planning Branch of the Ceylon Electricity Board and served as a Project Leader with Chulalongkorn University, Bangkok, Thailand. He is currently a Senior Lecturer with the University of Queensland (UQ), Brisbane, Australia. Prior to joining UQ, he was an Associate Professor with the Asian Institute of Technology, Bangkok, Thailand. His research interests are the integration of renewable energy in power systems and power system stability and dynamics.

Kwang Y. Lee (F'01) received the B.S. degree in electrical engineering from Seoul National University, Seoul, Korea, in 1964, the M.S. degree in electrical engineering from North Dakota State University, Fargo, in 1968, and the Ph.D. degree in system science from Michigan State University, East Lansing, MI, USA, in 1971.

He has been on the faculties of Michigan State, Oregon State, University of Houston, Penn State, and Baylor University, where he is a Professor and Chair of Electrical and Computer Engineering. His current research interests include power system control, operation and planning, and intelligent system techniques, and their application to power system and power plant control.

Dr. Lee has served as an editor of the IEEE TRANSACTIONS ON ENERGY CONVERSION and an associate editor of the IEEE TRANSACTIONS ON NEURAL NETWORKS.